ATLAS NOTE

ATLAS-CONF-2016-038

30th July 2016

Search for direct top squark pair production in events with a Z boson, b-jets and missing transverse momentum in $\sqrt{s} = 13$ TeV pp collisions with the ATLAS detector

The ATLAS Collaboration

Abstract

A search for direct top squark pair production resulting in events with at least three leptons, including a same-flavour opposite-sign pair with invariant mass compatible with that of Z boson, b-quark jets and missing transverse momentum is presented. The analysis is performed using proton-proton collision data at $\sqrt{s} = 13$ TeV collected with the ATLAS detector at the LHC in 2015-2016 corresponding to an integrated luminosity of 13.3 fb^{-1}. The results are interpreted in models featuring direct pair production of the heavier top squark $\tilde{t}_2$ decaying to the lighter top squark $\tilde{t}_1$ via $\tilde{t}_2 \rightarrow Z\tilde{t}_1$.

1 Introduction

Supersymmetry (SUSY) [1–6] is one of the most studied extensions of the Standard Model (SM). It predicts new bosonic partners for the existing fermions and fermionic partners for the known bosons. If R-parity is conserved [7], SUSY particles are produced in pairs and the lightest supersymmetric particle (LSP) is stable, providing a possible dark matter candidate. To address the SM hierarchy problem [8–11], TeV-scale masses are required [12, 13] for the supersymmetric partners of the gluons (gluinos, $\tilde{g}$) and top squark chirality states, left-handed stop ($\tilde{t}_{\mathrm{L}}$) and right-handed stop ($\tilde{t}_{\mathrm{R}}$) [14, 15]. The SUSY partners of the charged (neutral) Higgs and electroweak gauge bosons mix to form the mass eigenstates known as charginos, $\tilde{\chi}^{\pm}_{l}$, $l = 1, 2$ (neutralinos, $\tilde{\chi}^{0}_{m}$, $m = 1, \ldots, 4$) where the increasing index denotes increasing mass. The scalar partners of right-handed and left-handed quarks, $\tilde{q}_{\mathrm{R}}$ and $\tilde{q}_{\mathrm{L}}$, mix to form two mass eigenstates, $\tilde{q}_1$ and $\tilde{q}_2$, with $\tilde{q}_1$ defined to be the lighter of the two.

Searches for direct pair production of the lightest top squark mass eigenstate ($\tilde{t}_1$) have been performed by the ATLAS [16–18] and CMS [19–24] collaborations. Although the pair production of $\tilde{t}_1$ has a cross section larger than that of the heaviest top squark mass eigenstate ($\tilde{t}_2$), and their decays properties can be similar, searches for the latter can provide additional sensitivity in regions where the coverage of $\tilde{t}_1$ searches is limited. Searches for $\tilde{t}_1 \to t\tilde{\chi}^0_1$ have little sensitivity to scenarios where the lightest stop is only slightly heavier than the sum of the masses of the top quark and the LSP, due to the similarities in kinematics with SM top pair production ($t\bar{t}$). Sensitivity in that region of the mass parameter space can be achieved by considering the $\tilde{t}_2$ pair production decaying via $\tilde{t}_2 \to Z\tilde{t}_1$, as illustrated in Figure 1. This signal can be discriminated from the $t\bar{t}$ background by requiring a same-flavour opposite-sign lepton pair originating from the Z boson decay and the presence of a third lepton. Searches for $\tilde{t}_2$ were performed in the LHC Run-1 [25, 26]. Sensitivity to direct $\tilde{t}_2$ pair production can be obtained with this three-lepton signature even in models where additional decay modes of the $\tilde{t}_2$, such as $\tilde{t}_2 \to t\tilde{\chi}^0_1$ or via the lightest Higgs boson (H) in $\tilde{t}_2 \to H\tilde{t}_1$, are significant [25]. This note presents the results of a $\tilde{t}_2$ search at $\sqrt{s} = 13$ TeV using the data collected by the ATLAS experiment [27] in proton–proton (pp) collisions during 2015 and 2016.

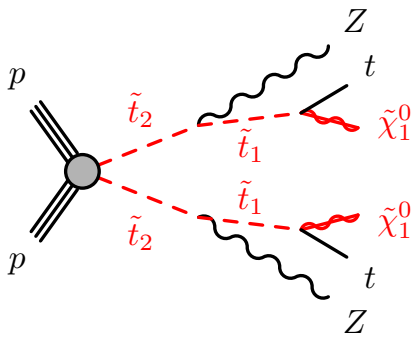

Figure 1: Diagram of the $\tilde{t}_2$ pair production process with $\tilde{t}_2 \to Z\tilde{t}_1$ and $\tilde{t}_1 \to t\tilde{\chi}^0_1$ decays considered in this analysis.

2 ATLAS detector

The ATLAS experiment [27] is a multi-purpose particle detector with a forward-backward symmetric cylindrical geometry and nearly 4π coverage in solid angle.[1] The interaction point is surrounded by an inner detector (ID), a calorimeter system, and a muon spectrometer.

The ID provides precision tracking of charged particles for pseudorapidities $|\eta| < 2.5$ and is surrounded by a superconducting solenoid providing a 2 T axial magnetic field. It consists of pixel and silicon-microstrip detectors inside a transition radiation tracker. One significant upgrade for the $\sqrt{s} = 13$ TeV running period is the presence of the Insertable B-Layer [28], an additional pixel layer close to the interaction point, which provides high-resolution hits at small radius to improve the tracking performance.

In the pseudorapidity region $|\eta| < 3.2$, high-granularity lead/liquid-argon (LAr) electromagnetic (EM) sampling calorimeters are used. A steel/scintillator tile calorimeter measures hadron energies for $|\eta| < 1.7$. The endcap and forward regions, spanning $1.5 < |\eta| < 4.9$, are instrumented with LAr calorimeters for both the EM and hadronic energy measurements.

The muon spectrometer consists of three large superconducting toroids with eight coils each, a system of trigger and precision-tracking chambers, which provide triggering and tracking capabilities in the ranges $|\eta| < 2.4$ and $|\eta| < 2.7$, respectively.

A two-level trigger system is used to select events [29]. The first-level trigger is implemented in hardware and uses a subset of the detector information. This is followed by the software-based High-Level Trigger stage, which can run offline reconstruction and calibration software, reducing the event rate to about 1 kHz.

3 Dataset and simulated event samples

The data were collected by the ATLAS detector during 2015 with a peak instantaneous luminosity of $L = 5.2 \times 10^{33}$ cm^{-2}s^{-1}, and during 2016 with a peak instantaneous luminosity of $L = 1.1 \times 10^{34}$ cm^{-2}s^{-1}, with a mean number of additional pp interactions per bunch crossing (pile-up) in the dataset of $\langle\mu\rangle = 14$ in 2015 and $\langle\mu\rangle = 22$ in 2016. Data quality requirements are applied to ensure that all sub-detectors were operating at nominal conditions, and that LHC beams were in stable-collision mode. The integrated luminosity of the resulting dataset is 13.3 fb^{-1} with an uncertainty of $\pm 2.9\%$. The luminosity and its uncertainty are derived following a methodology similar to that detailed in Ref. [30] from a preliminary calibration of the luminosity scale using a pair of x–y beam separation scans performed in August 2015 and June 2016.

Monte Carlo (MC) simulated event samples are used to aid in the estimation of the background from SM processes and to model the SUSY signal. Diboson processes with four charged leptons (ℓ), three charged leptons and one neutrino, or two charged leptons and two neutrinos are simulated using the Sherpa v2.1.1 generator [31], and are described in detail in Ref. [32]. The matrix elements contain the WW, WZ and

[1] ATLAS uses a right-handed coordinate system with its origin at the nominal interaction point (IP) in the centre of the detector and the z-axis along the beam pipe. The x-axis points from the IP to the centre of the LHC ring, and the y-axis points upward. Cylindrical coordinates (r, ϕ) are used in the transverse plane, ϕ being the azimuthal angle around the beam pipe. The pseudorapidity is defined in terms of the polar angle θ as $\eta = -\ln\tan(\theta/2)$. Rapidity is defined as $y = 0.5 \ln\left[(E + p_z)/(E - p_z)\right]$ where E denotes the energy and p_z is the component of the momentum along the beam direction.

ZZ processes and all other diagrams with four or six electroweak vertices (such as same-electric-charge W boson production in association with two jets, $W^{\pm}W^{\pm}jj$). Fully leptonic triboson processes (WWW, WWZ, WZZ and ZZZ) with up to six charged leptons are also simulated using Sherpa v2.1.1 and described in Ref. [32]. The 4ℓ and $2\ell + 2\nu$ processes are calculated at next-to-leading order (NLO) for up to one additional parton; final states with two and three additional partons are calculated at leading order (LO). The $WWZ \to 4\ell + 2\nu$ or $2\ell + 4\nu$ processes are calculated at LO with up to two additional partons. The $3\ell + 1\nu$ process is calculated at NLO and up to three extra partons at LO using the Comix [33] and OpenLoops [34] matrix element generators and merged with the Sherpa parton shower [35] using the ME+PS@NLO prescription [36]. The $WWZ/WZZ \to 3\ell + 3\nu$, $ZZZ \to 6\ell + 0\nu$, $4\ell + 2\nu$ or $2\ell + 4\nu$ processes are calculated with the same configuration but with up to only two extra partons at LO. The CT10 [37] parton distribution function (PDF) set is used for all Sherpa samples in conjunction with a dedicated tuning of the parton shower parameters developed by the Sherpa authors. The generator cross-sections (at NLO for most of the processes) are used when normalising these backgrounds.

Samples of $t\bar{t}V$ (with $V = W$ and Z, including non-resonant Z/γ^* contributions) and $t\bar{t}WW$ production are generated at LO with MadGraph5_aMC@NLO [38] v2.2.2 interfaced to the Pythia 8.186 [39] parton shower model, with up to two ($t\bar{t}W$), one ($t\bar{t}Z$) or no ($t\bar{t}WW$) extra partons included in the matrix element; they are described in detail in Ref. [40]. MadGraph5_aMC@NLO is also used to simulate the tZ, tWZ, $t\bar{t}t\bar{t}$ and $t\bar{t}t$ processes. The A14 set of tuned parameters (tune) [41] is used together with the NNPDF23LO PDF set [42]. The $t\bar{t}W$, $t\bar{t}Z$, $t\bar{t}WW$ and $t\bar{t}t\bar{t}$ events are normalised to their NLO cross-section [38] while the generator cross-section is used for tZ, tWZ and $t\bar{t}t$.

Production of a Higgs boson in association with a $t\bar{t}$ pair is simulated using MadGraph5_aMC@NLO [38] v2.2.2 interfaced to Herwig 2.7.1 [43]. The UEEE5 underlying-event tune is used together with the CTEQ6L1 [44] (matrix element) and CT10 [37] (parton shower) PDF sets. Simulated samples of SM Higgs boson production in association with a W or Z boson are produced with Pythia 8.186, using the A14 tune and the NNPDF23LO PDF set. For normalisation purposes, cross-sections calculated at NLO [45] are assumed.

The signal is modelled with a simplified model [46–48] featuring direct $\tilde{t}_2$ pair production, with all SUSY particles decoupled except for the $\tilde{t}_2$, $\tilde{t}_1$ and $\tilde{\chi}_1^0$, assumed to be the LSP. The only decays included in this model are $\tilde{t}_2 \to Z\tilde{t}_1$ and $\tilde{t}_1 \to t\tilde{\chi}_1^0$. The mass of the top quark is fixed at 172.5 GeV. The mass difference between the lighter stop and the neutralino is set to 180 GeV, a region not excluded by previous searches for $\tilde{t}_1$ with mass greater than 191 GeV [16]. Signal samples are generated from LO matrix elements with up to two extra partons, using the MadGraph5_aMC@NLO v2.2.3 generator interfaced to Pythia 8.186 with the A14 tune for the modelling of the SUSY decay chain, parton showering, hadronisation and the description of the underlying event. Parton luminosities are provided by the NNPDF23LO PDF set. Jet–parton matching is realised following the CKKW-L prescription [49], with a matching scale set to one quarter of the pair-produced superpartner mass. Signal cross-sections are calculated to NLO in the strong coupling constant, adding the resummation of soft gluon emission at next-to-leading-logarithmic accuracy (NLO+NLL) [50–54]. The nominal cross-section and the uncertainty are taken from an envelope of cross-section predictions using different PDF sets and factorisation and renormalisation scales, as described in Ref. [55].

In all MC samples, except those produced by Sherpa, the EvtGen v1.2.0 program [56] is used to model the properties of the bottom and charm hadron decays. To simulate the effects of additional pp collisions in the same and nearby bunch crossings, additional interactions are generated using the soft QCD processes of Pythia 8.186 with the A2 tune [57] and the MSTW2008LO PDF [58], and overlaid onto each simulated

hard scatter event. The Monte Carlo samples are reweighted so that the distribution of the number of reconstructed vertices matches the distribution observed in the data.

The MC samples are processed through an ATLAS detector simulation [59] based on GEANT4 [60] or, in the case of $t\bar{t}t$ and the SUSY signal samples, a fast simulation using a parameterisation of the calorimeter response and GEANT4 for the other parts of the detector [61]. All MC samples are reconstructed in the same manner as the data.

4 Event selection

Candidate events are required to have a reconstructed vertex [62] with at least two associated tracks with $p_{\mathrm{T}} > 400$ MeV. The vertex with the highest scalar sum of the squared transverse momentum of the associated tracks is considered to be the primary vertex of the event.

Electron candidates are reconstructed from isolated electromagnetic calorimeter energy deposits matched to ID tracks and are required to have $|\eta| < 2.47$, a transverse momentum $p_{\mathrm{T}} > 10\,\mathrm{GeV}$, and to pass a loose likelihood-based identification requirement [63, 64]. The likelihood input variables include measurements of calorimeter shower shapes and of track properties from the ID.

Muon candidates are reconstructed in the region $|\eta| < 2.5$ from muon spectrometer tracks matching ID tracks. Candidate muons must have $p_{\mathrm{T}} > 10\,\mathrm{GeV}$ and must pass the medium identification requirements defined in Ref. [65], based on the number of hits in the different ID and muon spectrometer subsystems, and on the significance of the charge to momentum ratio q/p [65].

Jets are reconstructed from three-dimensional energy clusters in the calorimeter [66] with the anti-k_t jet clustering algorithm [67] with a radius parameter $R = 0.4$. Only jet candidates with $p_{\mathrm{T}} > 30\,\mathrm{GeV}$ and $|\eta| < 2.5$ are considered as selected jets in the analysis. Jets are calibrated as described in Ref. [68]. In order to reduce the effects of pileup, for jets with $p_{\mathrm{T}} < 60\,\mathrm{GeV}$ and $|\eta| < 2.4$ a significant fraction of the tracks associated with each jet must have an origin compatible with the primary vertex, as defined by the jet vertex tagger [69]. Furthermore, for all jets the expected average energy contribution from pileup clusters is subtracted according to the jet area [68].

Identification of jets containing b-hadrons (b-tagging) is performed with the MV2c10 algorithm, a multivariate discriminant making use of track impact parameters and reconstructed secondary vertices [70, 71]. A requirement is chosen corresponding to a 77% average efficiency obtained for b-jets in simulated $t\bar{t}$ events. To compensate for differences between data and MC simulation in the b-tagging efficiencies and mis-tag rates, correction factors are applied to the simulated samples [71].

Jet candidates within $\Delta R = \sqrt{(\Delta y)^2 + (\Delta\phi)^2} < 0.2$ of a lepton candidate are discarded, unless the jet has a value of the MV2c10 discriminant larger than the value corresponding to approximately 85% b-tagging efficiency, in which case the lepton is discarded since it is likely originating from a semileptonic b-hadron decay. Any remaining electron candidate within $\Delta R < 0.4$ of a non-pileup jet, and any muon candidate within $\Delta R < \min\{0.4, 0.04 + p_{\mathrm{T}}(\ell)/10\,\mathrm{GeV}\}$ of a non-pileup jet is discarded. In the latter case, if the jet has fewer than three associated tracks or the muon p_{T} has more than $0.5p_{\mathrm{T}}^{\mathrm{jet}}$ and than $0.7\sum p_{\mathrm{T}}^{\mathrm{jet\ tracks}}$, the muon is retained and the jet is discarded instead to avoid inefficiencies for high-energy muons undergoing significant energy loss in the calorimeter. Any muon candidate reconstructed with ID and calorimeter information only that shares an ID track with an electron candidate is removed. Finally, any electron candidate sharing an ID track with the remaining muon candidates is also removed.

Signal electrons must satisfy the *medium* likelihood-based identification requirement as defined in [63, 64]. Signal electrons (muons) must fulfill the requirement of having a significance of the transverse impact parameter with respect to the reconstructed primary vertex, d_0, of $|d_0|/\sigma(d_0) < 5(3)$ and have a $p_{\mathrm{T}} > 20\,\mathrm{GeV}$. The track associated to the signal leptons must have a longitudinal impact parameter with respect to the reconstructed primary vertex, z_0, satisfying $|z_0 \sin\theta| < 0.5$ mm. Isolation requirements are applied to both the signal electrons and muons. The scalar sum of the p_{T} of tracks within a variable-size cone around the lepton, excluding its own track, must be less than 6% of the lepton p_{T}. The track isolation cone radius for electrons (muons) $\Delta R_\eta = \sqrt{(\Delta\eta)^2 + (\Delta\phi)^2}$ is given by the smaller of $\Delta R_\eta = 10\ \mathrm{GeV}/p_{\mathrm{T}}$ and $\Delta R_\eta = 0.2\,(0.3)$, that is, a cone of size $0.2\,(0.3)$ at low p_{T} but narrower for high-p_{T} leptons. In addition, in the case of electrons the energy of calorimeter energy clusters in a cone of $\Delta R_\eta = 0.2$ around the electron (excluding the deposition from the electron itself) must be less than 6% of the electron p_{T}.

The missing transverse momentum vector, whose magnitude is denoted by $E_{\mathrm{T}}^{\mathrm{miss}}$, is defined as the negative vector sum of the transverse momenta of all identified physics objects (electrons, photons, muons, jets) and an additional soft term. The soft term is constructed from all tracks that are not associated with any physics object, and which are associated with the primary vertex. In this way, the $E_{\mathrm{T}}^{\mathrm{miss}}$ is adjusted for the best calibration of the jets and the other identified physics objects above, while maintaining pileup independence in the soft term [72, 73].

Events are accepted if they pass an online selection (trigger) requiring either two electrons, two muons or an electron and a muon. The trigger-level requirements on the p_{T} of the leptons involved in the trigger decision are looser than those applied offline to ensure that trigger efficiencies are constant in the relevant phase space. Events are discarded if they contain any jet failing basic quality selection criteria that reject detector noise and non-collision backgrounds [74]

Simulated events are corrected to account for minor differences in the signal lepton trigger, reconstruction, identification and isolation efficiencies between data and MC simulation.

Events of interest are selected if they contain at least three signal leptons, with at least one same-flavour opposite-sign lepton pair whose invariant mass is compatible with the Z boson mass ($76.2 < m_{\ell\ell} < 106.2$ GeV). To maximise the sensitivity in different regions of the mass parameter space, three overlapping signal regions (SRs) are defined as shown in Table 1, with requirements on the p_{T} of the leading lepton and jet, the number of jets (n_{jets}) and b-jets ($n_{\mathrm{b-jets}}$), $E_{\mathrm{T}}^{\mathrm{miss}}$, and the transverse momentum of the same-flavour opposite-sign lepton pair forming the Z boson candidate ($p_{\mathrm{T}}^{\ell\ell}$). Signal region "L" (SRL) is designed to improve the sensitivity for compressed spectra ($m_{\tilde{t}_2} \gtrsim m_{\tilde{\chi}_1^0} + m_t$) without cutting on $p_{\mathrm{T}}^{\ell\ell}$ and with softer jet p_{T} requirements. Signal region "H" (SRH) is optimized for large mass splitting between the $\tilde{t}_2$ and $\tilde{\chi}_1^0$, where the Z boson in the $\tilde{t}_2 \to Z\tilde{t}_1$ decay is boosted, and large $p_{\mathrm{T}}^{\ell\ell}$ and leading jet p_{T} are required. Signal region "E" (SRE) covers the intermediate case, featuring slightly softer kinematic requirements.

5 Background estimation

The dominant SM background contribution to the SRs is expected to be the production of top-quark pairs in association with a Z boson ($t\bar{t}Z$), with minor contribution from diboson production (mainly WZ) and background containing fake and non-prompt leptons (mainly $t\bar{t}$). The normalisation of the main backgrounds ($t\bar{t}Z$, diboson) is obtained by fitting the yield to the observed data in a background dominated control region (CR), then extrapolating this yield to the SRs as described below. Other background sources

Table 1: Definition of the signal regions used in the analysis (see text for details).

Var/Region	SRL	SRH	SRE
$m_{\ell\ell}$ [GeV]	76.2–106.2	76.2–106.2	76.2–106.2
Leading lepton p_{T} [GeV]	> 40	> 40	> 40
Leading jet p_{T} [GeV]	> 60	> 100	> 80
$n_{\mathrm{b-jets}}$	≥ 1	≥ 1	≥ 1
n_{jets}	≥ 6	≥ 5	≥ 5
$E_{\mathrm{T}}^{\mathrm{miss}}$ [GeV]	> 100	> 100	> 100
$p_{\mathrm{T}}^{\ell\ell}$ [GeV]	–	> 200	> 100

($t\bar{t}W$, $t\bar{t}H$ and rare SM processes), which provide a sub-dominant contribution to the SRs, are determined from MC simulation only.

The fake and non-prompt lepton background is estimated from data with a method similar to that described in Refs. [75, 76]. Two types of lepton identification criteria are defined for this evaluation: "tight", corresponding to signal leptons described above, and "loose", corresponding to candidate electrons and muons described in Section 4. Since, as shown by simulation studies, the leading lepton is prompt in the SRs, the method makes use of the number of observed events with the second and third leading lepton being loose-loose, loose-tight, tight-loose and tight-tight in each region. The probability for prompt leptons passing the loose selection criteria to also pass the tight selection is measured on data using a $Z \to \ell\ell$ ($\ell = e, \mu$) enriched sample. The equivalent probability for fake or non-prompt leptons is measured using events with one electron and one muon with the same charge. The number of events with one or two fake or non-prompt leptons is calculated from these probabilities and the number of observed events with loose and tight leptons. The modelling of the fake and non-prompt lepton background is validated in events passing a selection similar to the SRs, but removing the $E_{\mathrm{T}}^{\mathrm{miss}}$ and inverting the $m_{\ell\ell}$ requirements. Figure 2 shows the jet multiplicity and $p_{\mathrm{T}}^{\ell\ell}$ for such events.

The two dedicated control regions for $t\bar{t}Z$ (CRTZ) and diboson (CRVV) backgrounds are defined as shown in Table 2. To ensure orthogonality with the SRs, $E_{\mathrm{T}}^{\mathrm{miss}} < 100$ GeV is required in CRTZ, while a b-jet veto is applied in CRVV.

Table 2: Definition of the control regions used in the analysis.

Var/Region	CRTZ	CRVV
$m_{\ell\ell}$ [GeV]	76.2–106.2	76.2–106.2
Leading lepton p_{T} [GeV]	> 40	> 40
Leading jet p_{T} [GeV]	> 60	> 60
$n_{\mathrm{b-jets}}$	≥ 1	0
$n_{\mathrm{jets}}(p_{\mathrm{T}} > 30$ GeV)	≥ 3	≥ 3
$E_{\mathrm{T}}^{\mathrm{miss}}$ [GeV]	< 100	–

Table 3 shows the observed and expected yields in the two CR for each background source, and Figure 3

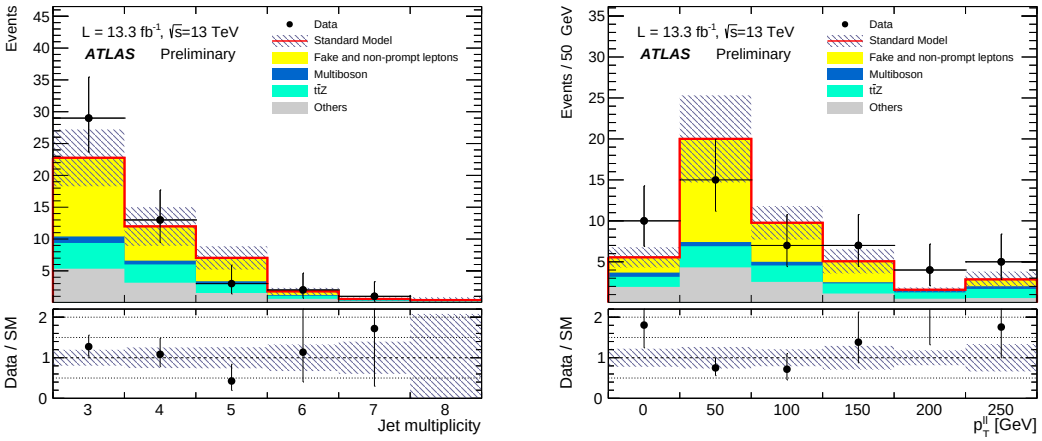

Figure 2: Jet multiplicity (left) and $p_{\mathrm{T}}^{\ell\ell}$ (right) for events with at least 3 jets, one b-jet and $m_{\ell\ell}$ outside of the 76.2–106.2 GeV window for an integrated luminosity of 13.3 fb^{-1}. The contributions from all SM backgrounds are shown as a histogram stack; the bands represent the total uncertainty.

shows the n_{jet} distribution in these regions. The normalisations of the $t\bar{t}Z$ and diboson backgrounds are adjusted to match the observed number of events in the corresponding CR with a good agreement between the data and the background model.

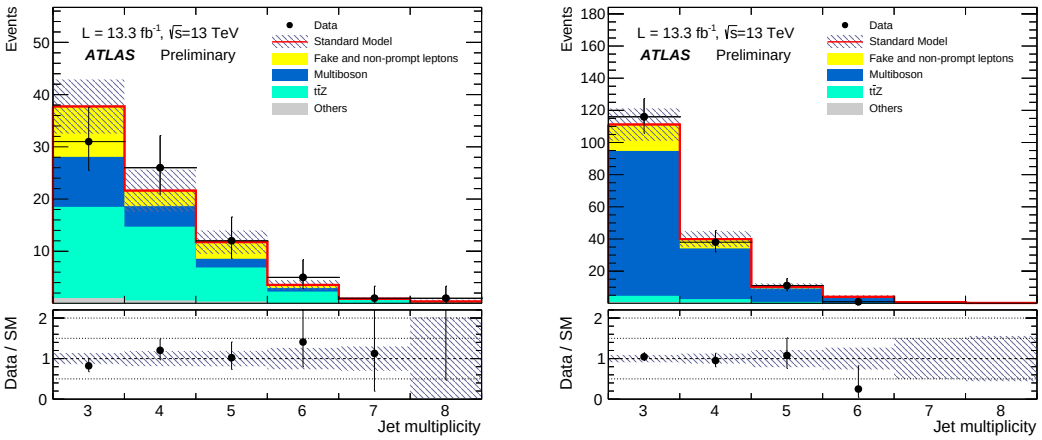

Figure 3: Jet multiplicity distributions in CRTZ (left) and CRVV (right) for an integrated luminosity of 13.3 fb^{-1}. The contributions from all SM backgrounds are shown as a histogram stack; the bands represent the total uncertainty.

For each signal region, a simultaneous "background" fit is performed to the number of events found in the two CRs, using the HistFitter package [77]. When setting 95% CL upper limits on the cross section of specific SUSY models, the simultaneous fits also include the observed yields in the SR. In each fit, the normalisations of the $t\bar{t}Z$ and diboson background contributions are allowed to float, while the fake and non-prompt lepton background is estimated from data and the other backgrounds are determined directly using the MC prediction. The normalisations for the $t\bar{t}Z$ and diboson backgrounds are found to be consistent with the theoretical predictions

Table 3: Background fit results for the CRs for an integrated luminosity of 13.3 fb^{-1}. The nominal expectations from MC simulation are given for comparison for those backgrounds ($t\bar{t}Z$, diboson) which are normalised to data. The "Others" category contains the contributions from associated production of $t\bar{t}$ with $W/H/WW/t/t\bar{t}$, as well as tZ, tWZ, WH, and ZH production. Combined statistical and systematic uncertainties are given. Events with fake or non-prompt leptons are estimated with the data-driven technique described in Section 5.

	CRVV	CRTZ
Observed events	166	76
Fitted background events	166 ± 13	75.8 ± 8.8
Fitted VV, VVV events	135 ± 15	16.0 ± 3.5
Fitted $t\bar{t}Z$ events	7.2 ± 2.3	41 ± 11
Fake and non-prompt lepton events	22.9 ± 8.0	16.4 ± 6.9
Fitted Others events	1.37 ± 0.50	2.25 ± 0.36
MC exp. VV, VVV events	133 ± 40	15.8 ± 5.4
MC exp. $t\bar{t}Z$ events	8.3 ± 1.4	47.4 ± 5.2

Systematic uncertainties in the MC simulation affect the ratio of the expected yields in the different regions and are taken into account to determine the uncertainty on the background prediction. The systematic uncertainties are described by nuisance parameters. Each uncertainty source is described by a single nuisance parameter, and all systematic uncertainty correlations between background processes and selections are taken into account. The list of systematic uncertainties considered in the fit is described in the next section.

6 Systematic Uncertainties

The primary sources of systematic uncertainties are related to: the jet energy scale (JES) and resolution (JER), and the theoretical and MC modelling uncertainties on $t\bar{t}Z$ and dibosons. The statistical uncertainty of the simulated event samples is taken into account as well. The effects of the systematic uncertainties is evaluated for all signal samples and background processes. Since the normalisation of the dominant background processes is extracted in dedicated control regions, the systematic uncertainties only affect the extrapolation to the signal regions in these cases.

The JES and JER uncertainties are derived as a function of the p_{T} and η of the jet, as well as of the pileup conditions and the jet flavour composition of the selected jet sample. They are determined using a combination of simulated and data samples, through measurements of the jet response asymmetry in dijet, Z+jet and γ+jet events [78]. Uncertainties associated to the modeling of the b-tagging efficiencies for b, c and light-flavor jets [79, 80] are also considered.

The systematic uncertainties related to the modelling of $E_{\mathrm{T}}^{\mathrm{miss}}$ in the simulation are estimated by propagating the uncertainties on the energy and momentum scale of each of the physics objects, as well as the uncertainties on the soft term resolution and scale [73].

Other detector-related systematic uncertainties, such as those on lepton reconstruction efficiency, energy scale, energy resolution and on the modelling of the trigger [64, 65], have been found to have a small impact on the results.

The uncertainties on the MC modelling of dibosons background are estimates by varying the renormalisation, factorisation and resummation scales used to generate the samples [32]. For $t\bar{t}Z$, the predictions from the MadGraph5_aMC@NLO and Sherpa generators are compared, and the uncertainties related to the choice of the renormalisation and factorisation scales are assessed by varying the corresponding generator parameters up and down by a factor of two around their nominal values [40], .

The cross-sections used to normalise the MC samples are varied according to the uncertainty on the cross-section calculation, that is, 6% for diboson, 13% for $t\bar{t}W$ and 12% $t\bar{t}Z$ production [38]. For $t\bar{t}WW$, tZ, tWZ, $t\bar{t}H$, $t\bar{t}t$, $t\bar{t}t\bar{t}$, and tribosons production processes, which constitute a small background, a 50% uncertainty on the event yields is assumed.

Systematic uncertainties are assigned to the fake and non-prompt lepton background estimate to account for potentially different compositions (heavy flavour, light flavour or conversions) between the signal and control regions, as well as the contamination from prompt leptons in the regions used to measure the probabilities for loose fake and non-prompt leptons to pass the tight signal criteria.

7 Results

Figure 4 shows the $E_{\mathrm{T}}^{\mathrm{miss}}$ distributions after applying all the selection criteria of the SR except that on $E_{\mathrm{T}}^{\mathrm{miss}}$. Table 4 shows the observed and expected yields in the two SRs for each background source, which are estimated as described in Section 5. Data agree with the SM background expectation within uncertainties.

Table 5 shows upper limits (at the 95% CL) on the visible new physics cross section $\langle \epsilon\sigma \rangle_{\mathrm{obs}}^{95}$, defined as the product of the production cross section, acceptance and efficiency. The HistFitter framework [77], which utilises a profile-likelihood-ratio test statistics [81], is used to compute the exclusion limits with the CL_s prescription [82] considering the full background estimation and luminosity uncertainties and assuming that the signal does not contaminate the CRs.

Model-dependent limits are also set on specific classes of SUSY models. For each signal hypothesis, the background fit is re-done taking into account the signal contamination in the CRs, which is found to be below 5% for signal models close to the Run-1 exclusion limits. The limit for each signal region is obtained by comparing the observed event count with that expected from SM background plus SUSY signal processes. All uncertainties on the SM expectation are considered, including those which are correlated between signal and background (for instance jet energy scale uncertainties) and all, except theoretical cross-section uncertainties (PDF and scale), on the signal expectation. Since the three SRs are not orthogonal, only the SR with best expected sensitivity is used to for each signal point. "Observed limits" are calculated from the observed SR event yields for the nominal signal cross section. "Expected limits" are calculated by setting the nominal event yield in each SR to the corresponding mean expected background.

Limits are shown for a class of simplified models in which only pair-produced $\tilde{t}_2$ decaying with 100% branching ratio into the $\tilde{t}_1$ and Z boson, with $\tilde{t}_1 \rightarrow t\tilde{\chi}_1^0$ are considered. Figure 5 shows the limits in the

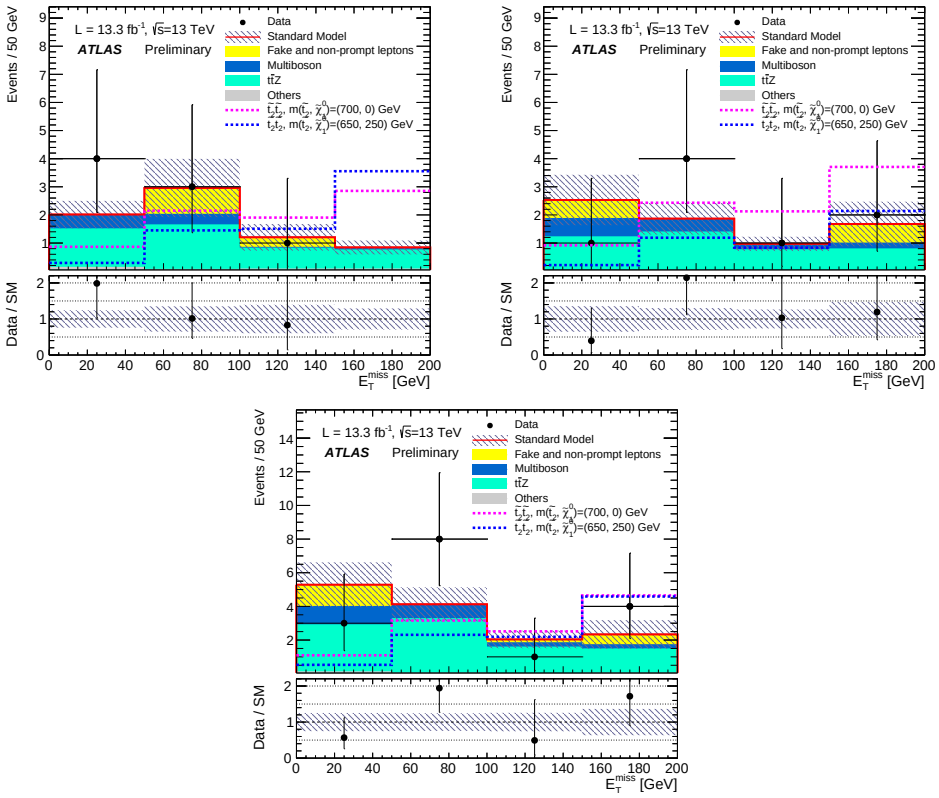

Figure 4: $E_{\mathrm{T}}^{\mathrm{miss}}$ distribution for events passing all the signal candidate selection requirements, except that on $E_{\mathrm{T}}^{\mathrm{miss}}$, for SRL (top left), SRH (top right) and SRE (bottom). The contributions from all SM backgrounds are shown; the bands represent the total uncertainty. The expected distributions for signal models with $m(\tilde{t}_2) = 700$ GeVand $m(\tilde{\chi}_1^0) = 0$ GeV and $m(\tilde{t}_2) = 650$ GeVand $m(\tilde{\chi}_1^0) = 250$ GeV are also shown as dashed lines.

$\tilde{t}_2$–$\tilde{\chi}_1^0$ mass plane, excluding $\tilde{t}_2$ squark masses up to 740 GeV at 95% CL for a neutralino of 70–100 GeV and neutralino mass up to 270 GeV are excluded for $\tilde{t}_2$ squark masses below 650 GeV.

Table 4: Background fit results for the three SRs for an integrated luminosity of 13.3 fb^{-1}. The nominal expectations from MC simulation are given for comparison for those backgrounds ($t\bar{t}Z$, diboson) which are normalised to data. The "Others" category contains the contributions from associated production of $t\bar{t}$ with $W/H/WW/t/t\bar{t}$, as well as tZ, tWZ, WH, and ZH production. Combined statistical and systematic uncertainties are given. Events with fake or non-prompt leptons are estimated with the data-driven technique described in Section 5. The observed events and the total (constrained) background are the same by construction. Uncertainties on the predicted background event yields are quoted as symmetric except where the negative error reaches down to zero predicted events, in which case the negative error is truncated.

	SRE	SRL	SRH
Observed events	5	1	3
Fitted bkg events	4.2 ± 1.1	2.05 ± 0.63	2.48 ± 0.82
Fitted VV, VVV events	0.51 ± 0.20	0.10 ± 0.07	0.40 ± 0.15
Fitted $t\bar{t}Z$ events	2.99 ± 0.90	1.42 ± 0.47	1.55 ± 0.47
Fake and non prompt lepton events	$0.59^{+0.70}_{-0.59}$	$0.34^{+0.39}_{-0.34}$	$0.50^{+0.65}_{-0.50}$
Fitted Others events	0.12 ± 0.06	0.19 ± 0.06	0.04 ± 0.03
MC exp. VV, VVV events	0.50 ± 0.24	0.09 ± 0.08	0.39 ± 0.19
MC exp. $t\bar{t}Z$ events	3.45 ± 0.50	1.64 ± 0.33	1.79 ± 0.28
$\tilde{t}_2\,\tilde{t}_2$ $m(\tilde{t}_2, \tilde{t}_1, \tilde{\chi}_1^0) = (700, 180, 0)$ GeV events	7.17 ± 0.77	4.76 ± 0.69	5.83 ± 0.83
$\tilde{t}_2\,\tilde{t}_2$ $m(\tilde{t}_2, \tilde{t}_1, \tilde{\chi}_1^0) = (650, 430, 250)$ GeV events	6.78 ± 0.97	5.1 ± 1.1	2.98 ± 0.93

Table 5: Signal model-independent 95% CL upper limits on the visible cross section ($\langle\epsilon\sigma\rangle^{95}_{\text{obs}}$), the visible number of signal events (S^{95}_{obs}) and the number of signal events (S^{95}_{exp}) given the expected number of background events (and $\pm 1\sigma$ excursions on the expectation).

Signal channel	$\langle\epsilon\sigma\rangle^{95}_{\text{obs}}$[fb]	S^{95}_{obs}	S^{95}_{exp}
SRE	0.53	7.1	$6.1^{+2.2}_{-1.6}$
SRL	0.29	3.8	$4.1^{+2.0}_{-0.4}$
SRH	0.43	5.8	$5.1^{+2.0}_{-1.1}$

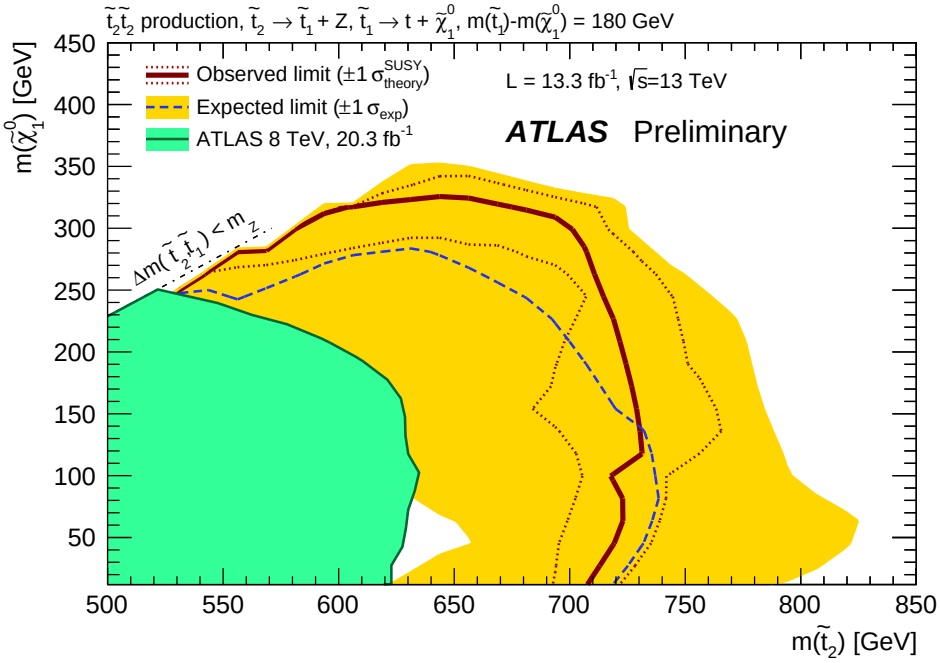

Figure 5: Exclusion limits at 95% CL from the analysis of 13.3 fb^{-1} of 13 TeV collision data on the masses of the $\tilde{t}_2$ and $\tilde{\chi}_1^0$, for a fixed $m(\tilde{t}_1) - m(\tilde{\chi}_1^0) = 180$ GeV and assuming BR($\tilde{t}_2 \to Z\tilde{t}_1$) = 1. The dashed line and the shaded band are the expected limit and its $\pm 1\sigma$ uncertainty, respectively. The thick solid line is the observed limit for the central value of the signal cross section. The expected and observed limits do not include the effect of the theoretical uncertainties on the signal cross section. The dotted lines show the effect on the observed limit when varying the signal cross section by $\pm 1\sigma$ of the theoretical uncertainty. The shaded green area shows the observed exclusion from the ATLAS $\sqrt{s} = 8$ TeV analysis [25].

8 Conclusion

This note reports a search for the heavy top squark eigenstate ($\tilde{t}_2$) pair production in final states containing a leptonic Z boson candidate plus an additional third lepton and large missing transverse momentum, based on a 13.3 fb^{-1} dataset of $\sqrt{s} = 13$ TeV proton-proton collisions recorded by the ATLAS experiment at the LHC in 2015 and 2016. Good agreement has been found between the observed events in the data and the expected SM yields.

Results are interpreted in the context of simplified models characterised by the decay chain $\tilde{t}_2 \to Z\tilde{t}_1$ with $\tilde{t}_1 \to t\tilde{\chi}_1^0$ and the mass difference between $\tilde{t}_1$ and $\tilde{\chi}_1^0$ slightly larger than the top mass. Parameter space regions up to $m_{\tilde{t}_2} < 730$ GeV and $m_{\tilde{\chi}_1^0} < 325$ GeV are excluded at 95% confidence level. These results extend the region of supersymmetric parameter space excluded by previous LHC searches.

References

[1] Yu. A. Golfand and E. P. Likhtman,
Extension of the Algebra of Poincare Group Generators and Violation of P Invariance,
JETP Lett. **13** (1971) 323, [Pisma Zh. Eksp. Teor. Fiz.13,452(1971)].

[2] D. V. Volkov and V. P. Akulov, *Is the Neutrino a Goldstone Particle?*, Phys. Lett. **B46** (1973) 109.

[3] J. Wess and B. Zumino, *Supergauge Transformations in Four-Dimensions*, Nucl. Phys. **B70** (1974) 39.

[4] J. Wess and B. Zumino, *Supergauge Invariant Extension of Quantum Electrodynamics*, Nucl. Phys. **B78** (1974) 1.

[5] S. Ferrara and B. Zumino, *Supergauge Invariant Yang-Mills Theories*, Nucl. Phys. **B79** (1974) 413.

[6] A. Salam and J. A. Strathdee, *Supersymmetry and Nonabelian Gauges*, Phys. Lett. **B51** (1974) 353.

[7] G. R. Farrar and P. Fayet, *Phenomenology of the Production, Decay, and Detection of New Hadronic States Associated with Supersymmetry*, Phys. Lett. **B76** (1978) 575.

[8] N. Sakai, *Naturalness in Supersymmetric Guts*, Z. Phys. **C11** (1981) 153.

[9] S. Dimopoulos, S. Raby and F. Wilczek, *Supersymmetry and the Scale of Unification*, Phys. Rev. **D24** (1981) 1681.

[10] L. E. Ibanez and G. G. Ross, *Low-Energy Predictions in Supersymmetric Grand Unified Theories*, Phys. Lett. **B105** (1981) 439.

[11] S. Dimopoulos and H. Georgi, *Softly Broken Supersymmetry and SU(5)*, Nucl. Phys. **B193** (1981) 150.

[12] R. Barbieri and G. F. Giudice, *Upper Bounds on Supersymmetric Particle Masses*, Nucl. Phys. **B306** (1988) 63.

[13] B. de Carlos and J. A. Casas, *One loop analysis of the electroweak breaking in supersymmetric models and the fine tuning problem*, Phys. Lett. **B309** (1993) 320, arXiv: hep-ph/9303291.

[14] K. Inoue et al., *Aspects of Grand Unified Models with Softly Broken Supersymmetry*, Prog. Theor. Phys. **68** (1982) 927, [Erratum: Prog. Theor. Phys. **70** (1983) 330].

[15] J. R. Ellis and S. Rudaz, *Search for Supersymmetry in Toponium Decays*, Phys. Lett. **B128** (1983) 248.

[16] ATLAS Collaboration, *ATLAS Run 1 searches for direct pair production of third-generation squarks at the Large Hadron Collider*, Eur. Phys. J. **C75** (2015) 510, [Erratum: Eur. Phys. J.C76,no.3,153(2016)], arXiv: 1506.08616 [hep-ex].

[17] ATLAS Collaboration, *Search for top squarks in final states with one isolated lepton, jets, and missing transverse momentum in $\sqrt{s}$ = 13 TeV pp collisions with the ATLAS detector*, (2016), arXiv: 1606.03903 [hep-ex].

[18] ATLAS Collaboration, *Search for direct top squark pair production in final states with two leptons in $\sqrt{s}$ = 13 TeV pp collisions using 3.2 fb^{-1} of ATLAS data*, ATLAS-CONF-2016-009, 2016, URL: http://cdsweb.cern.ch/record/2139643.

[19] CMS Collaboration, *Search for top-squark pair production in the single-lepton final state in pp collisions at $\sqrt{s}$ = 8 TeV*, Eur. Phys. J. C **73** (2013) 2677, arXiv: 1308.1586 [hep-ex].

[20] CMS Collaboration, *Search for supersymmetry using razor variables in events with b-tagged jets in pp collisions at $\sqrt{s}$ = 8 TeV*, Phys. Rev. D **91** (2015) 052018, arXiv: 1502.00300 [hep-ex].

[21] CMS Collaboration, *Searches for supersymmetry using the M_{T2} variable in hadronic events produced in pp collisions at 8 TeV*, JHEP **05** (2015) 078, arXiv: 1502.04358 [hep-ex].

[22] CMS Collaboration, *Search for supersymmetry in events with soft leptons, low jet multiplicity, and missing transverse momentum in proton-proton collisions at $\sqrt{s}$=8 TeV*, Submitted to Phys. Lett. B (2015), arXiv: 1512.08002 [hep-ex].

[23] CMS Collaboration, *Search for direct pair production of scalar top quarks in the single- and dilepton channels in proton-proton collisions at $\sqrt{s}$=8 TeV*, Submitted to JHEP (2016), arXiv: 1602.03169 [hep-ex].

[24] CMS Collaboration, *A Search for Scalar Top Quark Production and Decay to All Hadronic Final States in pp Collisions at $\sqrt{s}$=8 TeV*, CMS-PAS-SUS-13-023, 2015, URL: https://cds.cern.ch/record/2044441.

[25] ATLAS Collaboration, *Search for direct top squark pair production in events with a Z boson, b-jets and missing transverse momentum in $\sqrt{s}$ = 8 TeV pp collisions with the ATLAS detector*, Eur. Phys. J. **C74** (2014) 2883, arXiv: 1403.5222 [hep-ex].

[26] CMS Collaboration, *Search for top-squark pairs decaying into Higgs or Z bosons in pp collisions at $\sqrt{s}$=8 TeV*, Phys. Lett. **B736** (2014) 371, arXiv: 1405.3886 [hep-ex].

[27] ATLAS Collaboration, *The ATLAS Experiment at the CERN Large Hadron Collider*, JINST **3** (2008) S08003.

[28] ATLAS Collaboration, *ATLAS Insertable B-Layer Technical Design Report*, CERN-LHCC-2010-013. ATLAS-TDR-19, 2010, URL: http://cds.cern.ch/record/1291633.

[29] ATLAS Collaboration, *2015 start-up trigger menu and initial performance assessment of the ATLAS trigger using Run-2 data*, ATL-DAQ-PUB-2016-001, 2016, URL: https://cds.cern.ch/record/2136007/.

[30] ATLAS Collaboration, *Improved luminosity determination in pp collisions at $\sqrt{s}$ = 7 TeV using the ATLAS detector at the LHC*, Eur. Phys. J. C **73** (2013) 2518, arXiv: 1302.4393 [hep-ex].

[31] T. Gleisberg et al., *Event generation with SHERPA 1.1*, JHEP **02** (2009) 007, arXiv: 0811.4622 [hep-ph].

[32] ATLAS Collaboration, *Multi-Boson Simulation for 13 TeV ATLAS Analyses*, ATL-PHYS-PUB-2016-002, 2016, URL: http://cds.cern.ch/record/2119986.

[33] T. Gleisberg and S. Höche, *Comix, a new matrix element generator*, JHEP **12** (2008) 039, arXiv: 0808.3674 [hep-ph].

[34] F. Cascioli, P. Maierhofer and S. Pozzorini, *Scattering Amplitudes with Open Loops*, Phys. Rev. Lett. **108** (2012) 111601, arXiv: 1111.5206 [hep-ph].

[35] S. Schumann and F. Krauss, *A Parton shower algorithm based on Catani-Seymour dipole factorisation*, JHEP **03** (2008) 038, arXiv: 0709.1027 [hep-ph].

[36] S. Höche et al., *QCD matrix elements + parton showers: The NLO case*, JHEP **04** (2013) 027, arXiv: 1207.5030 [hep-ph].

[37] H.-L. Lai et al., *New parton distributions for collider physics*, Phys.Rev. **D82** (2010) 074024, arXiv: 1007.2241 [hep-ph].

[38] J. Alwall et al., *The automated computation of tree-level and next-to-leading order differential cross sections, and their matching to parton shower simulations*, JHEP **07** (2014) 079, arXiv: 1405.0301 [hep-ph].

[39] T. Sjöstrand, S. Mrenna and P. Z. Skands, *A Brief Introduction to PYTHIA 8.1*, Comput. Phys. Commun. **178** (2008) 852, arXiv: 0710.3820 [hep-ph].

[40] ATLAS Collaboration, *Modelling of the $t\bar{t}H$ and $t\bar{t}V$ ($V = W, Z$) processes for $\sqrt{s} = 13$ TeV ATLAS analyses*, ATL-PHYS-PUB-2015-022, 2016, URL: http://cds.cern.ch/record/2120826.

[41] ATLAS Collaboration, *ATLAS Pythia8 tunes to 7 TeV data*, ATL-PHYS-PUB-2014-021, 2014, URL: http://cds.cern.ch/record/1966419.

[42] R. D. Ball et al., *Parton distributions with LHC data*, Nucl. Phys. **B867** (2013) 244, arXiv: 1207.1303 [hep-ph].

[43] G. Corcella et al., *HERWIG 6: An Event generator for hadron emission reactions with interfering gluons (including supersymmetric processes)*, JHEP **01** (2001) 010, arXiv: hep-ph/0011363.

[44] J. Pumplin et al., *New generation of parton distributions with uncertainties from global QCD analysis*, JHEP **07** (2002) 012, arXiv: hep-ph/0201195.

[45] LHC Higgs Cross Section Working Group, *Handbook of LHC Higgs Cross Sections: 2. Differential Distributions*, CERN-2012-002 (CERN, Geneva, 2012), arXiv: 1201.3084 [hep-ph].

[46] J. Alwall et al., *Searching for Directly Decaying Gluinos at the Tevatron*, Phys. Lett. **B666** (2008) 34, arXiv: 0803.0019 [hep-ph].

[47] J. Alwall, P. Schuster and N. Toro, *Simplified Models for a First Characterization of New Physics at the LHC*, Phys. Rev. **D79** (2009) 075020, arXiv: 0810.3921 [hep-ph].

[48] D. Alves, *Simplified Models for LHC New Physics Searches*, J. Phys. **G39** (2012) 105005, ed. by N. Arkani-Hamed et al., arXiv: 1105.2838 [hep-ph].

[49] L. Lönnblad and S. Prestel, *Matching Tree-Level Matrix Elements with Interleaved Showers*, JHEP **03** (2012) 019, arXiv: 1109.4829 [hep-ph].

[50] W. Beenakker et al., *Squark and gluino production at hadron colliders*, Nucl.Phys. **B492** (1997) 51, arXiv: hep-ph/9610490.

[51] A. Kulesza and L. Motyka, *Threshold resummation for squark-antisquark and gluino-pair production at the LHC*, Phys.Rev.Lett. **102** (2009) 111802, arXiv: 0807.2405 [hep-ph].

[52] A. Kulesza and L. Motyka, *Soft gluon resummation for the production of gluino-gluino and squark-antisquark pairs at the LHC*, Phys.Rev. **D80** (2009) 095004, arXiv: 0905.4749 [hep-ph].

[53] W. Beenakker et al., *Soft-gluon resummation for squark and gluino hadroproduction*, JHEP **12** (2009) 041, arXiv: 0909.4418 [hep-ph].

[54] W. Beenakker et al., *Squark and gluino hadroproduction*, Int.J.Mod.Phys. **A26** (2011) 2637, arXiv: 1105.1110 [hep-ph].

[55] M. Krämer et al., *Supersymmetry production cross sections in pp collisions at* $\sqrt{s}$ = 7 *TeV*, (2012), arXiv: 1206.2892 [hep-ph].

[56] D. J. Lange, *The EvtGen particle decay simulation package*, Nucl. Instrum. Meth. **A462** (2001) 152.

[57] ATLAS Collaboration, *Summary of ATLAS Pythia 8 tunes*, ATLAS-PHYS-PUB-2012-003, 2012, URL: http://cdsweb.cern.ch/record/1474107.

[58] A. D. Martin et al., *Parton distributions for the LHC*, Eur. Phys. J. **C63** (2009) 189, arXiv: 0901.0002 [hep-ph].

[59] ATLAS Collaboration, *The ATLAS Simulation Infrastructure*, Eur.Phys.J. **C70** (2010) 823, arXiv: 1005.4568 [physics.ins-det].

[60] S. Agostinelli et al., *GEANT4: A Simulation toolkit*, Nucl.Instrum.Meth. **A506** (2003) 250.

[61] ATLAS Collaboration, *The simulation principle and performance of the ATLAS fast calorimeter simulation FastCaloSim*, ATL-PHYS-PUB-2010-013, 2010, URL: http://cds.cern.ch/record/1300517.

[62] ATLAS Collaboration, *Vertex Reconstruction Performance of the ATLAS Detector at*$\sqrt{s}$ = 13 *TeV*, ATL-PHYS-PUB-2015-026, 2015, URL: http://cdsweb.cern.ch/record/2037717.

[63] ATLAS Collaboration, *Electron efficiency measurements with the ATLAS detector using the 2012 LHC proton-proton collision data*, ATLAS-CONF-2014-032, 2014, URL: http://cds.cern.ch/record/1706245.

[64] ATLAS Collaboration, *Electron identification measurements in ATLAS using* $\sqrt{s}$ *= 13 TeV data with 50 ns bunch spacing*, ATL-PHYS-PUB-2015-041, 2015, URL: http://cds.cern.ch/record/2048202.

[65] ATLAS Collaboration, *Muon reconstruction performance in early Run II*, ATL-PHYS-PUB-2015-037, 2015, URL: http://cds.cern.ch/record/2047831.

[66] ATLAS Collaboration, *Topological cell clustering in the ATLAS calorimeters and its performance in LHC Run 1*, (2016), arXiv: 1603.02934 [hep-ex].

[67] M. Cacciari, G. P. Salam and G. Soyez, *The anti-kt jet clustering algorithm*, JHEP **04** (2008) 063, arXiv: 0802.1189 [hep-ph].

[68] ATLAS Collaboration, *Jet Calibration and Systematic Uncertainties for Jets Reconstructed in the ATLAS Detector at* $\sqrt{s}$ = 13 *TeV*, ATL-PHYS-PUB-2015-015, 2015, URL: http://cds.cern.ch/record/2028594.

[69] ATLAS Collaboration, *Tagging and suppression of pileup jets with the ATLAS detector*, ATLAS-CONF-2014-018, 2014, URL: http://cdsweb.cern.ch/record/1700870.

[70] ATLAS Collaboration, *Performance of b-Jet Identification in the ATLAS Experiment*, (2015), arXiv: 1512.01094 [hep-ex].

[71] ATLAS Collaboration, *Expected performance of the ATLAS b-tagging algorithms in Run-2*, ATL-PHYS-PUB-2015-022, 2015, URL: http://cds.cern.ch/record/2037697.

[72] ATLAS Collaboration, *Performance of missing transverse momentum reconstruction for the ATLAS detector in the first proton-proton collisions at at* $\sqrt{s}$*= 13 TeV*, ATL-PHYS-PUB-2015-027, 2015, URL: http://cds.cern.ch/record/2037904.

[73] ATLAS Collaboration, *Expected performance of missing transverse momentum reconstruction for the ATLAS detector at $\sqrt{s} = 13$ TeV*, ATL-PHYS-PUB-2015-023, 2015, URL: http://cds.cern.ch/record/2037700.

[74] ATLAS Collaboration, *Data-Quality Requirements and Event Cleaning for Jets and Missing Transverse Energy Reconstruction with the ATLAS Detector in Proton–Proton Collisions at a Center-of-Mass Energy of $\sqrt{s} = 7$ TeV*, ATLAS-CONF-2010-038, 2010, URL: http://cdsweb.cern.ch/record/1277678.

[75] ATLAS collaboration, *Measurement of the top quark-pair production cross section with ATLAS in pp collisions at $\sqrt{s} = 7$ TeV*, Eur. Phys. J. **C 71** (2011) 1577, arXiv: 1012.1792 [hep-ex].

[76] ATLAS collaboration, *Measurement of the top quark pair production cross section in pp collisions at $\sqrt{s} = 7$ TeV in dilepton final states with ATLAS*, Phys. Lett. **B 707** (2012) 459, arXiv: 1108.3699 [hep-ex].

[77] M. Baak et al., *HistFitter software framework for statistical data analysis*, Eur. Phys. J. **C75** (2015) 153, arXiv: 1410.1280 [hep-ex].

[78] ATLAS Collaboration, *Jet Calibration and Systematic Uncertainties for Jets Reconstructed in the ATLAS Detector at $\sqrt{s} = 13$ TeV*, ATL-PHYS-PUB-2015-015, 2015, URL: https://cds.cern.ch/record/2037613.

[79] ATLAS Collaboration, *Calibration of b-tagging using dileptonic top pair events in a combinatorial likelihood approach with the ATLAS experiment*, ATLAS-CONF-2014-004, 2014, URL: http://cdsweb.cern.ch/record/1664335.

[80] ATLAS Collaboration, *Calibration of the performance of b-tagging for c and light-flavour jets in the 2012 ATLAS data*, ATLAS-CONF-2014-046, 2014, URL: http://cdsweb.cern.ch/record/1741020.

[81] G. Cowan et al., *Asymptotic formulae for likelihood-based tests of new physics*, Eur. Phys. J. **C71** (2011) 1554, [Erratum: Eur. Phys. J. **C73** (2013) 2501], arXiv: 1007.1727 [physics.data-an].

[82] A. L. Read, *Presentation of search results: the CL s technique*, Journal of Physics G: Nuclear and Particle Physics **28** (2002) 2693.

Appendix

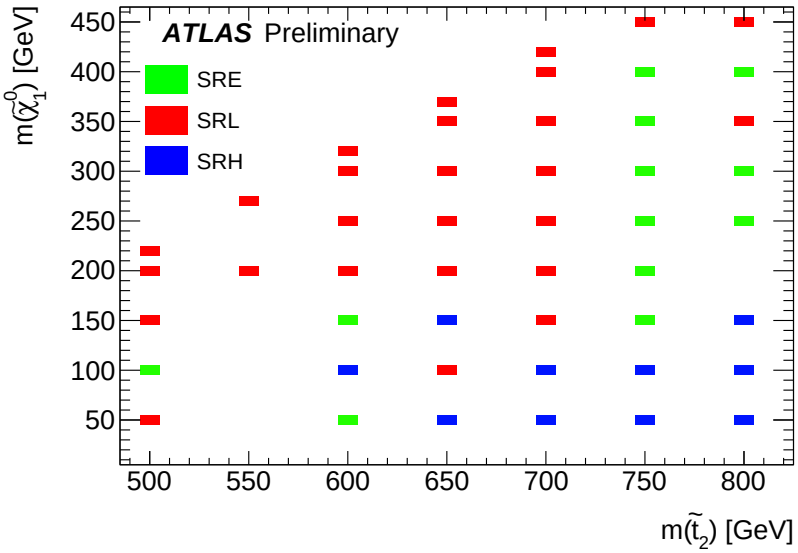

Figure 6: Illustration of the best expected signal region per signal grid point for the $\tilde{t}_2 \to Z\tilde{t}_1$ with $\tilde{t}_1 \to t\tilde{\chi}_1^0$ model. This mapping is used for the final combined exclusion limits.

Table 6: Number of signal events selected at different stages for some scenarios in the $\tilde{t}_2 \to Z\tilde{t}_1$ with $\tilde{t}_1 \to t\tilde{\chi}_1^0$ model. Only the statistical uncertainties are displayed.

	$m(\tilde{t}_2, \tilde{t}_1, \tilde{\chi}_1^0) = (700, 180, 0)$ GeV		$m(\tilde{t}_2, \tilde{t}_1, \tilde{\chi}_1^0) = (650, 430, 250)$ GeV	
Selection	Raw events	Events for 13.3 fb^{-1}	Raw events	Events for 13.3 fb^{-1}
Total	23422	891.7	29080	1423.7
3 baseline leptons	1453	55.3 ± 2.0	1805	85.4 ± 2.7
Trigger	1304	49.2 ± 1.4	1587	76.7 ± 1.9
≥3 signal leptons	659	24.8 ± 1.0	714	34.5 ± 1.3
≥1 OSSF pair	645	24.3 ± 1.0	692	33.4 ± 1.3
Lead lepton $p_{\mathrm{T}} > 40$ GeV	645	24.3 ± 1.0	691	33.4 ± 1.3
$\lvert m_{\ell\ell} - m_Z \rvert < 15$ GeV	583	21.9 ± 0.9	636	30.8 ± 1.2
$n_{b\text{-jet}} > 0$	516	19.4 ± 0.9	559	27.1 ± 1.1
Leading jet $p_{\mathrm{T}} > 60$ GeV	514	19.3 ± 0.9	541	26.2 ± 1.1
$E_{\mathrm{T}}^{\mathrm{miss}}$ >100 GeV	336	12.6 ± 0.7	398	19.4 ± 1.0
SRL	137	4.8 ± 0.4	113	5.1 ± 0.5
SRE	206	7.2 ± 0.5	152	6.8 ± 0.6
SRH	167	5.8 ± 0.4	66	3.0 ± 0.4